On the Behavior of Friction in Lubricated Point Contact With Provision for Surface Roughness

H. Sojoudi

M. M. Khonsari[1]
Dow Chemical Endowed Chair in Rotating Machinery
Fellow ASME
e-mail: khonsari@me.lsu.edu

Department of Mechanical Engineering,
Louisiana State University,
2508 Patrick Taylor Hall,
Baton Rouge, LA 70803

This paper presents a simple approach to predict the behavior of friction coefficient in the sliding lubricated point contact. Based on the load-sharing concept, the total applied load is supported by the combination of hydrodynamic film and asperity contact. The asperity contact load is determined in terms of maximum Hertzian pressure in the point contact while the fluid hydrodynamic pressure is calculated through adapting the available numerical solutions of elastohydrodynamic lubrication (EHL) film thickness formula for smooth surfaces. The simulations presented cover the entire lubrication regime including full-film EHL, mixed-lubrication, and boundary-lubrication. The results of friction, when plotted as a function of the sum velocity, result in the familiar Stribeck-type curve. The simulations are verified by comparing the results with published experimental data. A parametric study is conducted to investigate the influence of operating condition on the behavior of friction coefficient. A series of simulations is performed under various operating conditions to explore the behavior of lift-off speed. An equation is proposed to predict the lift-off speed in sliding lubricated point contact, which takes into account the surface roughness. [DOI: 10.1115/1.4000306]

1 Introduction

Research in elastohydrodynamic lubrication (EHL) study added a new dimension when researchers turned their attention from rectangular to elliptical conjunctions in the early 1970s. This began in 1970 when Cheng [1] developed a Grubin type inlet analysis applicable to elliptical Hertzian contact. Later, Hamrock and Dowson [2] conducted a comprehensive study on EHL analysis of ball bearings where they showed that the theoretical features are in overall agreement with experiments. More recently, computational schemes that utilize multilevel solvers are extended for prediction of film thickness in lubricated elliptic contacts. The pressure and film thickness on the center-line of the contact are predicted accurately from an equivalent point contact analysis [3].

EHL research has progressively continued. Yet most of the published works are limited to "smooth" interacting surfaces where roughness and surface features are absent in the formulation. In fact, the classical analysis of elastic contact between two spheres as formulated and solved by Hertz pertains to smooth surfaces while engineering surfaces are rough. Therefore, when two mating surfaces are pressed together, most of the real contact occurs at the tips of the surface asperities. The asperities of mating surfaces behave like a spring as they interact under an applied load, so that contact is extended over a larger area than the contact between two smooth surfaces. Under a high applied load, the contact region in the central area is surrounded by a fringe in which only higher asperities are involved in contact. On the other hand, a reduction in the real contact area may occur due to light applied load where the asperities are not flattened; this may result in an increase in contact pressure due to asperity peak interaction of a rough surface. It is clear that the classical Hertzian analysis cannot hold for describing the contact of rough surfaces.

The elastic contact of rough spheres has been studied by several investigators. Greenwood and Tripp [4] extended the Hertzian theory of elastic contact to a number of discrete microcontacts in an attempt to find the real pressure distribution over the contact area. Yip and Venart [5] formulated the contact between curved rough bodies based on the assumptions that the roughness height distribution is Gaussian and that the deformation of the surface roughness is elastic while that due to waviness is fully plastic.

Zhu and Ai [6] presented a numerical solution for the EHL analysis of point contacts where they investigated the surface roughness effects on the average film thickness and the pressure peak. Hu and Zhu [7] proposed a new, simple, and robust numerical approach for the mixed EHL analysis of point contact. The system of equations and the numerical procedure are unified for a full coverage of all the lubrication regions including the full-film-, mixed-, and boundary-lubrications. A comprehensive study considering thermal effects is presented by Wang et al. [8]. This model deterministically calculates pressure and surface temperature by simultaneously solving a system of equations that govern the lubrication, elastic deformation, and thermal behaviors of a point contact. Simulations and measurements of sliding friction coefficient between rough surfaces in point contacts are performed by Wang et al. [9]. They used a full-scale deterministic solution of mixed-lubrication for the prediction of film thickness, pressure, and the area of real contact. The friction from asperity contact was determined in terms of the limiting shear stress while the fluid shear stress in the lubrication areas was calculated using different rheological models. Their simulations covered the entire lubrication regime including full-film EHL, mixed-lubrication, and boundary-lubrication. The results for friction plotted as a function of sliding velocity revealed a Stribeck-type behavior.

Most of the recent available efforts for predicting friction behavior in lubricated point contact require solving the Reynolds, deformation, load balance, and appropriate rheology equations simultaneously using an iterative procedure that is generally time consuming and often experiences computational sensitivity. The need for a simple and robust model capable of rapidly predicting the behavior of rough point contact still remains. To fulfill this need, a deterministic model for treating point contact problems is presented that implements the load-sharing concept pioneered by Johnson et al. [10]. The idea was first proposed by Gelinck and Schipper [11] in sliding lubricated line contact and then continued by Liu et al. [12] who investigated the effects of rheological behavior of the lubricant on the friction coefficient. Lu et al. [13] extended the idea further with experimental verification. Farron

[1]Corresponding author.

Contributed by the Tribology Division of ASME for publication in the JOURNAL OF TRIBOLOGY. Manuscript received July 9, 2009; final manuscript received September 23, 2009; published online November 12, 2009. Assoc. Editor: Michael D. Bryant.

and Schipper [14] applied this method to consider the starvation effect in lubricated line contact. A follow up study is performed by Akbarzadeh and Khonsari [15] who applied Johnson's load-sharing concept to lubrication analysis of gears. All of these publications are limited to the line contact.

Liu et al. [16] predicted the friction in point contact conjunctions based on load-sharing concept; however, their study is limited to heavy load operating conditions. They assumed that the asperity contact pressure is equal to Hertzian point contact pressure, which could be a rough estimation in highly loaded conditions. The objective of this study is to extend the EHL line contact method developed in Refs. [11–14] to sliding lubricated point contact and to provide a simple model, which is useful for control applications where rapid prediction and friction compensation are essential for instruments supported on ball bearings. For this purpose, a series of curve fits is developed that can be used for approximating pressure and real area of contact; the essential point is that the behavior of rough surfaces is determined assuming Gaussian statistical distribution of asperity heights subject to elastic deformation. Bair–Winer [17] model is adopted to describe the shear stress of the lubricant. The model and the solution algorithm are capable of predicting the friction behavior of lubricated rough point contact surfaces. The model is simple, but realistic and easily converges to the desired results. Rapid convergence and computational time for the prediction of friction coefficient in the entire range of operation are the beauty of the proposed model, making it useful in real-time applications.

2 Theoretical Development

2.1 Friction Expression. Based on Johnson's load-sharing concept, the total applied load F_T is supported by hydrodynamic lifting force F_H and asperity interacting force F_C.

$$F_T = F_H + F_C \tag{1}$$

Applying the load-sharing concept, the problem of solving the Reynolds, deformation, load balance, and rheological equations simultaneously can be easily replaced with the problem of the dry point contact and the problem of lubricated point contact. Using the relevant scaling factor for the hydrodynamic part γ_1 and asperity contact γ_2, Eq. (1) can be rewritten as

$$F_T = \frac{F_T}{\gamma_1} + \frac{F_T}{\gamma_2} \tag{2}$$

Similarly, the total friction force is the sum of two components

$$F_f = F_{f,H} + F_{f,C} \tag{3}$$

where $F_{f,H}$ is the hydrodynamic friction force given by the following expression:

$$F_{f,H} = \iint \tau_H dA_H \tag{4}$$

where τ_H represents the fluid shear stress and A_H is the contact area of the fluid.

The asperity contact friction is given by

$$F_{f,C} = \sum_{i=1}^{N} \iint \tau_{C_i} dA_{C_i} \tag{5}$$

where τ_{C_i} represents the contact shear stress of an individual asperity, A_{C_i} is the area of an individual asperity in contact, and N is the number of the asperities in contact.

The asperity friction may be written as the product of an average asperity friction coefficient f_c and the load carried by the asperities F_C. Therefore, we arrive at the following relation for the friction force:

$$F_{f,C} = f_C F_C \tag{6}$$

To determine the shear stress of hydrodynamic films, the traction model developed by Bair and Winer [17] is adopted. It is defined as

$$\eta^* = \eta \frac{1}{\lambda}(1 - e^{-\lambda}) \tag{7}$$

where

$$\lambda = \frac{\eta|\dot{\gamma}|}{\tau_L} \tag{8}$$

where $\dot{\gamma}$ is the shear stain rate and τ_L is the limiting shear stress, which is considered as a function of pressure described by

$$\tau_L = \tau_{L0} + \beta_0 p_m \tag{9}$$

where τ_{L0} is the limiting shear stress at the ambient pressure, β_0 is the slope of the limiting shear stress-pressure relation, and p_m is the mean pressure of Hertzian point contact.

The fluid traction force per unit length F_l is determined by integrating the shear stress

$$F_l = \int \tau dx = \int \eta^* \dot{\gamma} dx \tag{10}$$

Assuming the separation of two rough surfaces is constant and equal to central film thickness h_c, the fluid traction force then can be rewritten as

$$F_{f,H} = \tau_L(1 - e^{-\eta(u/h_c)/\tau_L}) \cdot \pi a^2 \tag{11}$$

where u is the effective velocity and a is the radius of point contact. According to Roelands's formula [18], the lubricated viscosity up to a certain elevated pressure is given by

$$\eta = \eta_0 \left(\frac{\eta_\infty}{\eta_0} \right)^{(1-(1+p_m/c_P)^Z)} \tag{12}$$

where η_0 is the oil viscosity at inlet temperature and η_∞ is 6.35×10^{-5} Pa s. The parameter Z represents the pressure-viscosity index as [19]

$$Z = \frac{\alpha}{[5.1 \times 10^{-9}(\ln \eta_0 + 9.67)]} \tag{13}$$

where α is the pressure-viscosity coefficient.

Another expression for the change in viscosity with pressure, often attributed to Barus [20], is of the following form:

$$\eta = \eta_0 e^{\alpha p_m} \tag{14}$$

Hence, the total friction coefficient can be obtained from

$$f = \frac{F_f}{F_T} = \frac{F_{f,H} + F_{f,C}}{F_T} \tag{15}$$

2.2 Governing EHL Equations. There are three basic equations for the EHL problem: Reynolds equation, the deformation equation, and the load balance. Nijenbanning et al. [3] developed an accurate relationship to predict the central film thickness based on numerical solution of the following equations:

$$\bar{h}_c = \{[\bar{h}_{RI}^{3/2} + (\bar{h}_{EI}^{-4} + \bar{h}_{00}^{-4})^{-3/8}]^{2s/3} + (\bar{h}_{RP}^{-8} + \bar{h}_{EP}^{-8})^{-s/8}\}^{1/s} \tag{16}$$

where

$$s = 1.5(1 + e^{[-1.2\bar{h}_{EI}/\bar{h}_{RI}]}) \tag{17}$$

with the following group of dimensionless parameters:

$$\bar{h}_{00} = 1.8D^{-1}$$

$$\bar{h}_{RI} = C_{RI}M^{-2}, \quad C_{RI} = 145(1 + 0.796D^{14/15})^{-15/7}D^{-1}$$

$$\bar{h}_{EI} = C_{EI} M^{-2/15}, \quad C_{EI} = 3.18(1 + 0.006 \ln D + 0.63D^{4/7})^{-14/25} D^{-1/15}$$

$$\bar{h}_{RP} = C_{RP} L^{2/3}, \quad C_{RP} = 1.29(1 + 0.691D)^{-2/3}$$

$$\bar{h}_{EP} = C_{EP} M^{-1/12} L^{3/4}, \quad C_{EP} = 1.48(1 + 0.006 \ln D + 0.63D^{4/7})^{-7/20} D^{-1/24} \tag{18}$$

The additional dimensionless parameters will be defined as follows:

$$M = WU_{\Sigma}^{-3/4}, \quad L = GU_{\Sigma}^{1/4}, \quad W = \frac{F}{E' R_x^2}, \quad G = \alpha E',$$

$$U_{\Sigma} = \frac{\eta_0 u}{E' R_x}, \quad \bar{h}_c = \bar{h}_{\text{cen}} U_{\Sigma}^{-1/2}, \quad \bar{h}_{\text{cen}} = h/R_x \tag{19}$$

The subscripts denote the following: *RI* is rigid-isoviscous, *RP* is rigid-piezoviscous, *EI* is elastic-isoviscous, and *EP* is elastic-piezoviscous.

In the mixed-lubrication regime the total pressure p_T is split into hydrodynamic pressure p_H and asperity contact pressure p_C. Therefore, the film thickness equation should be appropriately implemented according to Eqs. (2) and (3). This is done by writing $p_T = \gamma_1 p_H$. In Reynolds equation the pressure P is replaced with p_H whereas in deformation and load balance equations the total pressure is used. Replacing E' with E'/γ_1 and F_T with F_T/γ_1, the central film thickness for the mixed-lubrication in a point contact is expressed as

$$\bar{h}_c = \{[\bar{h}_{RI}^{3/2} \gamma_1^{9/4} + (\bar{h}_{EI}^{-4} \gamma_1^{-2/5} + \bar{h}_{00}^{-4})^{-3/8}]^{2s/3} + (\bar{h}_{RP}^{-8} \gamma_1^{4} + \bar{h}_{EP}^{-8} \gamma_1^{4})^{-s/8}\}^{1/s} \times \gamma_1^{1/2} \tag{20}$$

where

$$s = 1.5(1 + e^{[-1.2\gamma_1^{-7/5} \bar{h}_{EI}/\bar{h}_{RI}]}) \tag{21}$$

2.3 Asperity Contact Term. Quantitative analysis of dry point contact using the Greenwood and Williamson [21] model of a rough surface is applied to the point contact of spheres by Greenwood and Tripp [4]. The axisymmetric case can be simplified to the contact of smooth sphere of radius R with a nominally flat rough surface having a standard distribution of summit heights σ_s. The separation d between two rough, deformed surfaces is given by

$$d(r) = w_b(r) - y(r) = -y_0 + (r^2/2R) + w_b(r) \tag{22}$$

where w_b is the bulk displacement, $y(r)$ is the profile of the undeformed sphere relative to the data, and y_0 is its value at the center of the contact. Datum is taken at the mean level of the rough surface. The bulk compression w_b can be written as [4]

$$w_b(r) = \frac{4}{\pi E'} \int_0^a \frac{s}{s + r} p(s) K(k) ds \tag{23}$$

where $K(k)$ is the complete elliptic integral of the first kind with argument $k = 2(rs)^{1/2}/(r+s)$. Assuming that the asperities deform elastically, the effective pressure at radius r is found to be

$$p(r) = \frac{4}{3} n \sqrt{\beta} E' \int_d^{\infty} (z_s - d(r))^{3/2} e^{-(1/2) z_s^2} dz_s \tag{24}$$

where z_s is the height of the asperity summit above the data. Equations (22)–(24) are solved by Greenwood and Tripp [4] for the case of asperity heights with Gaussian distribution. Central film thickness is used to obtain the pressure in the surface asperities. In the present study, a series of curve fits is developed to relate the maximum asperity contact pressure, which occurs at the center of the point contact to the maximum Hertzian point contact. The result is given as follows:

$$\frac{p_c}{p_0} = a + be^{-\zeta} + \frac{c \ln(\mu)}{\mu} \tag{25}$$

The dimensionless parameters used in Eq. (25) are defined as

$$\zeta = \sigma_s \left(\frac{16 R E'^2}{9 F_T^2} \right)^{1/3} \tag{26}$$

$$\mu = \tfrac{8}{3} n \sigma_s (2R\beta)^{1/2} \tag{27}$$

where $a = 0.2342$, $b = 0.8189$, $c = -0.2720$, and p_0 represents the maximum Hertzian pressure for the point contact

$$p_0 = \left(\frac{3 F_T E'^2}{2\pi^3 R^2} \right)^{1/3} \tag{28}$$

p_c is the central contact pressure defined by Greenwood and Williamson [21] defined as

$$p_c = \frac{2}{3} n E' \beta^{1/2} \sigma_s^{3/2} F_{3/2}\left(\frac{h}{\sigma_s} \right) \tag{29}$$

where

$$F_{3/2}\left(\frac{h(x)}{\sigma_s} \right) = \frac{1}{\sqrt{2\pi}} \int_{h(x)/\sigma_s}^{\infty} \left(s - \frac{h(x)}{\sigma_s} \right)^{3/2} e^{-(1/2)s^2} ds \tag{30}$$

It is important to note that the sliding velocity affects the influence of deformed asperities in EHL contact; this effect is ignored in the present study. The results of the calculation for the asperity contact are adopted for the mixed-lubrication analogous to the hydrodynamic term. Thus, $p_T = \gamma_2 p_C$. The results for the mixed-lubrication then can be obtained by replacing E' with E'/γ_2, F_T with F_T/γ_2, and n with $n\gamma_2$. For the central pressure in a rough point contact these substitutions in Eqs. (25), (28), and (29) yield the following result:

$$\frac{2}{3} \bar{n} \bar{\sigma}_s^{\frac{3}{2}} \bar{F}_T F_{3/2}\left(\frac{\bar{h}_c - \bar{d}_d}{\bar{\sigma}_s} \right) = \left\{ a + be^{-\zeta} + \frac{c(\ln(\gamma_2) + \ln(\mu))}{\gamma_2 \mu} \right\} \frac{1}{\gamma_2} \tag{31}$$

with the following group of dimensionless parameters:

$$\bar{F}_T = \left(\frac{\pi^3 R^2 E'}{6 F_T} \right)^{1/3}$$

$$\bar{n} = nR\sqrt{R\beta}, \quad \bar{\sigma}_s = \frac{\sigma_s}{R}$$

$$\bar{h}_c = \frac{h_c}{R}, \quad \bar{d}_d = \frac{d_d}{R} \tag{32}$$

3 Solution Procedure

There are three unknowns (γ_1, γ_2, and h_c) associated in Eqs. (2), (20), and (31). An iteration method is utilized to solve this set of nonlinear equations. For a given steady velocity and load, an initial value for $\gamma_2 > 1$ is assumed and γ_1 is obtained using Eq. (2); then Eq. (20) is solved for the central film thickness h_c. Having the value for the central film thickness, the validity of Eq. (31) is checked. The iterations are continued until the error between two successive iterations falls below a specified tolerance value ($\varepsilon_T = 0.001$). This procedure is performed for the next sliding velocity. In the following simulations, general relations of film thickness for the contact of elliptical surfaces are reduced to the contact of spheres assuming $D = 1$ and $R_x = R_y = R$ results in $k = 1$. The computations are typically converged within 10 s predicting the Stribeck curve under given operating conditions.

Table 1 Input parameters for steady simulations and experiments [9]

Parameter	Value
n	1×10^{10} m^{-2}
β	2×10^{-6} m
σ_s	1.6×10^{-6} m
E'	2.19×10^{11} Pa
η_0	0.1756 Pa·s
R	0.0127 m
f_c	0.16
α	18.8×10^{-9} Pa^{-1}
β_0	0.05
τ_{L0}	2×10^{6} Pa

4 Results and Discussion

4.1 Verification. In order to verify the prediction of the model for the friction coefficient, we use the published experimental results by Wang et al. [9]. Their setup consists of a rotary flat sample in contact with a steel ball, which has a diameter of 25.4 mm. The contact zone is immersed in a lubricant reservoir. Two different sets of experiments were conducted: reciprocal mode and rotary mode. In this study, only the second category of the results is used for validation purposes. The tests were started from a low speed and then increased in a stepwise manner until the maximum speed was reached. At each speed the test lasted for 2 min to ensure that the steady-state condition is reached. The simulation is performed within the same speed range of the experiments reported in Table 3 of Ref. [9]. The input parameters for the simulations are reported in Table 1; these correspond to experimental values reported in Ref. [9]. According to Ref. [9], the experiments were repeated to investigate the reproducibility of the results. Four friction curves are measured on four samples whose σ_s have the same value of 1.6 μm. The density of asperities n and the average radius for the asperities β for the simulation are chosen so that $\Phi=\sigma_s n\beta$ is 0.032 and the best agreement with the experiments is reached. According to Greenwood and Williamson [21], for engineering surface, Φ typically varies between 0.03 and 0.05. It is also assumed that the Coulomb friction coefficient f_c for the asperity contact is 0.16.

Figure 1 shows the simulation result and the comparison with experiments reported in Ref. [9]. The simulation results are in good agreement with the experimental results of Wang et al. (Fig. 7 of Ref. [9]). The model predicts that the friction coefficient drops in the mixed-lubrication regime and increases slightly after the transition from mixed- to full-film-lubrication regime. The discrepancies between the simulations and experimental results can be, in part, attributed to simplifications in the model and the uncertainty in some of the input variables used in the simulations.

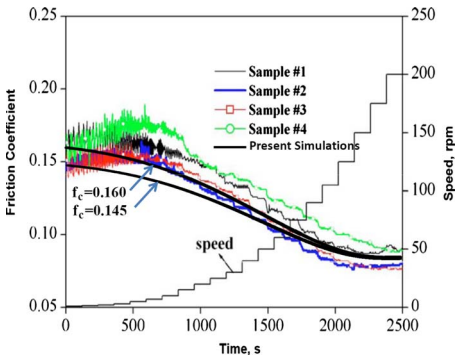

Fig. 1 Variation of the total friction coefficient (present simulations and experimental results [9])

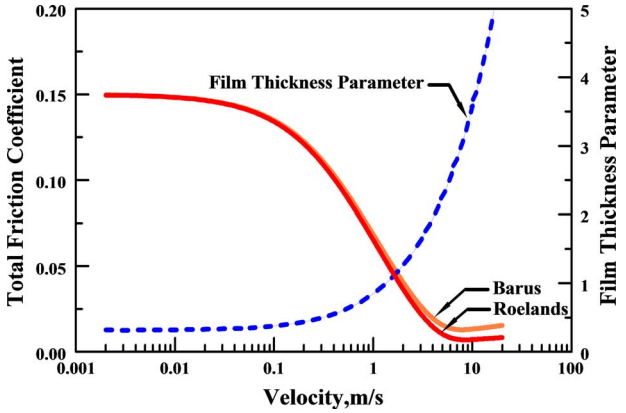

Fig. 2 The film thickness parameter and effect of pressure-viscosity relations on the total friction coefficient, F_T=40 N and η_0=0.01 Pa s

According to Ref. [9], while the overall trend remains the same, the inconsistency in samples each made individually in the machine shop results in different magnitudes for friction coefficient. Two different values are used in simulations; comparison of the results reveals that a change in the asperity friction coefficient results in a change in the predicted friction coefficient in the boundary- and mixed-lubrication regimes. Deviation of the friction coefficient becomes significant while approaching the boundary regime from the mixed-lubrication regime. In the full-film-lubrication regime, the contribution of asperities is nil and the two curves coincide.

4.2 Film Thickness Parameter. Figure 2 examines the variation of the film thickness parameter $\Lambda(\Lambda=h_c/\sigma_s)$ with velocity. The input parameters of the simulation are tabulated in Table 2. The results reveal that an increase in the film thickness parameter in the mixed-lubrication regime results in a decrease in the friction coefficient while there is a reverse influence in the full-film-lubrication regime. The film thickness parameter increases exponentially while the transition from the mixed- to the full-film-lubrication occurs.

The effect of pressure-viscosity relations on the total friction coefficient is also investigated. Roelands [18] and Barus's [20] pressure-viscosity relation is represented by Eqs. (12) and (14), respectively. As a result, the calculated friction coefficient in the boundary- and mixed-lubrication regimes is nearly identical using each of these rheological models. Near the transition from mixed to the hydrodynamic regime, Barus's model predicts a higher friction coefficient and that this trend continues in the hydrodynamic regime. Using these pressure-viscosity relations, the same trend is reported by Wang et al. [9]. It should be noted, however, that these

Table 2 Input parameters for parametric study simulations

Parameter	Value
n	5×10^{10} m^{-2}
β	10×10^{-6} m
σ_s	0.05×10^{-6} m
E'	2.19×10^{11} Pa
η_0	8×10^{-3} Pa s
R	0.01 m
f_c	0.15
α	9.4×10^{-9} Pa^{-1}
β_0	0.047
τ_{L0}	2.5×10^{6} Pa

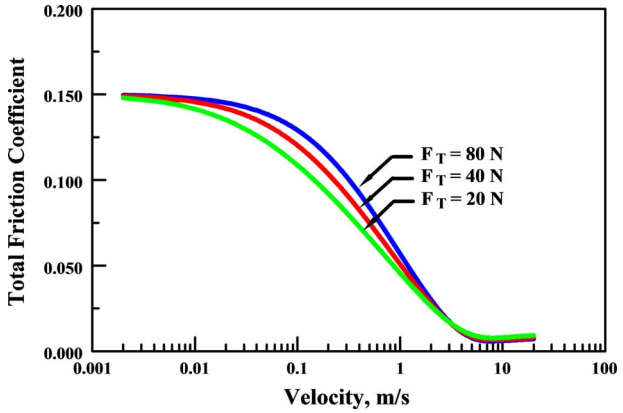

Fig. 3 Total friction coefficient as a function of velocity (load effect), $\eta_0=8\times10^{-3}$ Pa s

relationships best describe the viscosity at moderate values of pressures.

The results of a series of simulations are presented in Secs. 4.3–4.5 to investigate the influence of key operational parameters in a point contact configuration.

4.3 Effect of Load. Figure 3 shows the simulation results for the sliding lubrication of a smooth ball in contact with a rough flat surface. The curves for different applied loads show the deviation in the friction coefficient in three different regimes: boundary, mixed, and full. The physical explanation of the problem is interesting. In the boundary regime, increasing the applied load forces more asperities into contact; this results in higher coefficient of friction. The film thickness increases due to an increase in the sliding velocity when the operating regime initiates from the boundary-lubrication, passing through the mixed-lubrication, and ending in the full-lubrication.

The total friction coefficient is the combination of asperity contact friction and hydrodynamic friction. In the boundary regime and most part of the mixed regime, asperity contact friction is dominant while at the end of the mixed and whole part of the fluid-film regime, the traction associated with the fluid plays a dominant role. Comparison between Figs. 4(*a*) and 4(*b*) reveals the change in the behavior of asperity contact and hydrodynamic friction coefficient. In the boundary- and mixed-lubrication regimes, an increase in the applied load results in a greater asperity contact and friction coefficient rise. However, in the hydrodynamic regime, the trend is the opposite: An increase in the applied load causes a decrease in the film thickness and friction coefficient decreases. As the friction coefficient approaches to the end of the mixed regime, the contribution of hydrodynamic film in carrying the applied load becomes more pronounced. Therefore, due to the decrease in the hydrodynamic friction coefficient, the total friction coefficient will be reduced. This means that there is a point in the Stribeck curve in which the effect of a change in the applied load on the total friction coefficient changes. It is important to note that thermal effects are neglected.

4.4 Effect of Oil Inlet Viscosity. In Fig. 5 simulations correspond to three different lubricant inlet viscosities. It is clear that the changes in viscosity do not appreciably influence the friction coefficient in the boundary regime since friction is influenced largely by the lubricant's chemical composition.

Simulation results reveal how the behavior of friction coefficient in the mixed regime changes due to changes in the lubricant viscosity. The lower the viscosity, the greater is the possibility of metal-to-metal contact and, in turn, the higher friction coefficient becomes. In the full-lubrication regime, the friction coefficient is directly related to the viscosity. For a lower viscosity, the lubricant shear stress or friction coefficient is lower. Thus, the change in the

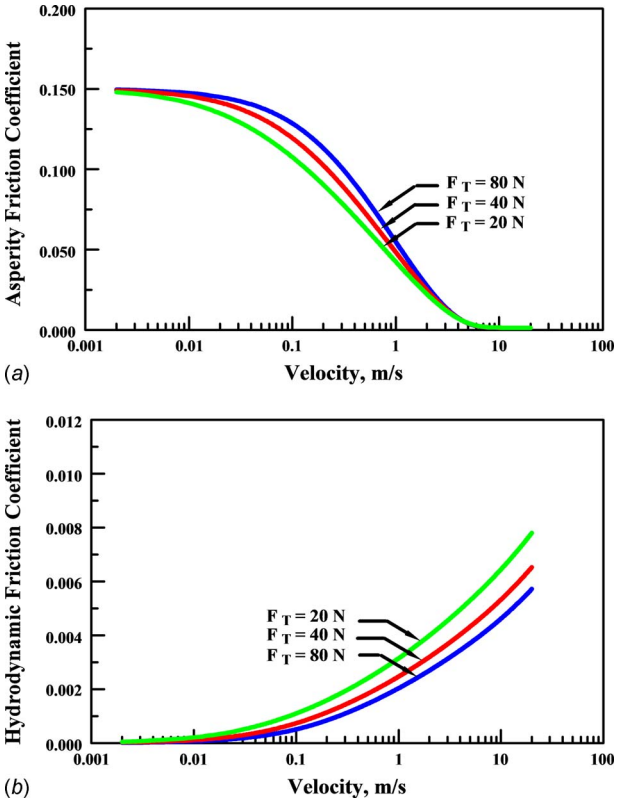

Fig. 4 Load effect on the friction coefficient, $\eta_0=8\times10^{-3}$ Pa s. (*a*) Asperity contact friction coefficient and (*b*) hydrodynamic friction coefficient.

viscosity has a different influence in different regimes. It is important to note that depending on the operating condition, the selection of the proper lubricant is important for lowering energy losses. It can be seen that the transition from mixed- to full-film-lubrication is postponed for a lubricant with lower viscosity.

4.5 Effect of Surface Roughness. In this section, the behavior of friction coefficient is predicted by investigating different surface roughnesses. There are three different parameters corresponding to the surface roughness: n, density of asperities; β, average radius of asperities; and σ_s, standard deviation of asperities. Simulations of different roughness parameters indicate that the change in standard deviation of asperities has a significant effect on the friction coefficient behavior. Simulation results for

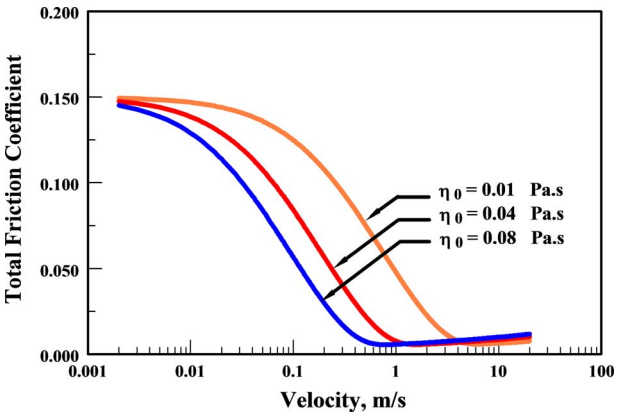

Fig. 5 Total friction coefficient as a function of velocity (lubricant viscosity effect), $F_T=20$ N

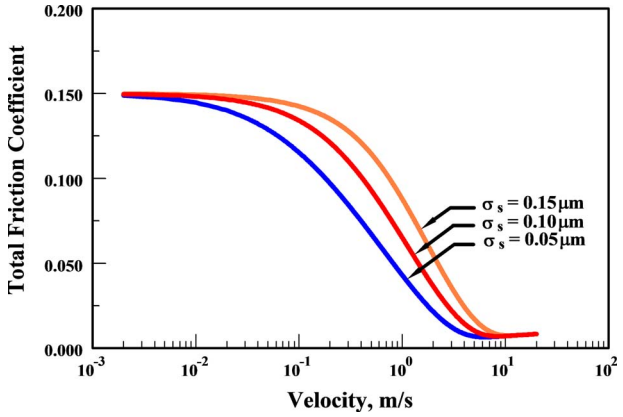

Fig. 6 Total friction coefficient as a function of velocity (roughness effect), $\eta_0=1\times10^{-2}$ Pa s and $F_T=40$ N

different standard deviations of surface roughness are presented in Fig. 6. For a rough surface, the film thickness required to fill out the separation between the asperities is higher. Therefore, under the same operating conditions, there will be more metal-to-metal contact for a rougher surface. This translates to higher values for the friction coefficient.

The results clearly indicate that the velocity in which transition from mixed- to full-lubrication regimes occurs is higher for a rougher surface, as intuitively expected. Since the influence of asperity contact is ignored in driving full-film-lubrication's equations, there is no difference in the total friction coefficient for different roughness values.

Figures 7(*a*) and 7(*b*) show the influence of surface roughness on the hydrodynamic and asperity contact scaling factors, respectively. It is clear that the hydrodynamic scaling factor decreases as the speed increases; this translates to an increase in contribution of hydrodynamic film in supporting the applied load while the reverse is true for the scaling factor associated with the asperity contact. Figures 7(*a*) and 7(*b*) reveal that an increase in the surface roughness decreases the asperity scaling factor and increases the hydrodynamic scaling factor.

Figure 8 shows the influence of other roughness parameters, n and β, on the behavior of friction coefficient. For a surface with a higher value for the surface roughness parameter Φ, the total friction coefficient is higher in the mixed-lubrication regime. Figure 8 reveals that under the conditions simulated, 25% increase in Φ may result in up to 12.5% increase in the total friction coefficient in the mixed-lubrication regime. However, for a fixed standard deviation of asperities σ_s, the influence of increase in the asperities' density n, is dominant compared to the increase in the average radius of asperities β. This behavior is depicted in Fig. 7. It is important to note that under the conditions simulated, the lift-off speed does not change significantly due to a constant value for σ_s.

5 Lift-Off Speed

The speed at which transition from mixed- to full-film-lubrication occurs is often referred to as the lift-off speed. This is the speed at which the friction coefficient attains its minimum value in the Stribeck curve. A series of simulation is conducted to investigate the influence of different input parameters on the lift-off speed. The influences of different operating conditions are lumped in the nondimensional parameters defined in the formulation of the problem. Using the simulation data in the regression analysis, the following equation is derived for the nondimensional lift-off speed:

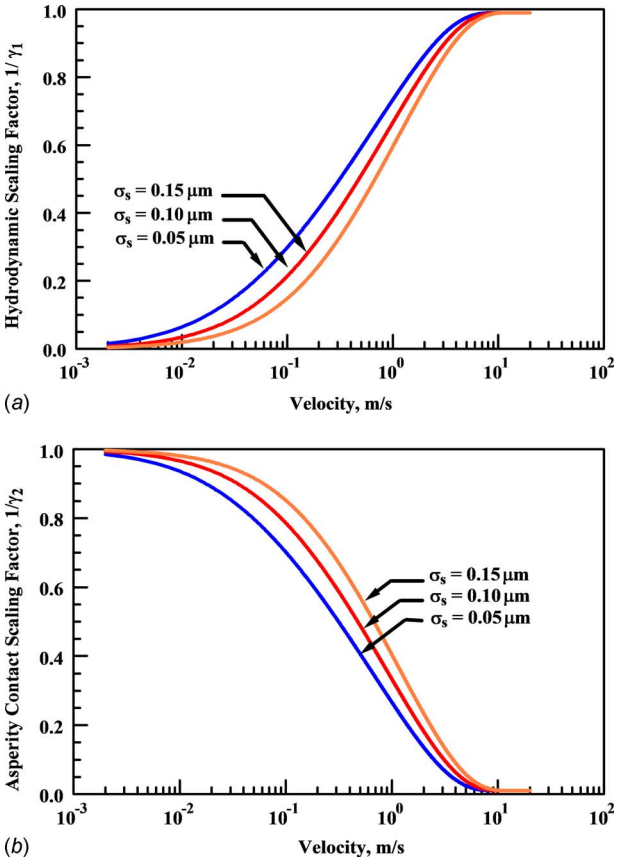

Fig. 7 (*a*) Hydrodynamic scaling factor γ_1 for different roughnesses, $\eta_0=1\times10^{-2}$ Pa s and $F_T=40$ N. (*b*) Asperity scaling factor γ_2 for different roughnesses, $\eta_0=1\times10^{-2}$ Pa s and $F_T=40$ N.

$$U_{\Sigma_{\text{lift-off}}} = 3.9053 \times 10^{-9} W^{0.01684} G^{-0.8247} \mu^{1.4953} \tag{33}$$

where $U_{\Sigma_{\text{lift-off}}} = \eta_0 u_{\text{lift-off}}/E'R$ and W, G, and μ are nondimensional load, material, and roughness parameters, respectively, defined in Sec. 2.

Given specific input parameters, lift-off speed $u_{\text{lift-off}}$ can be easily estimated. It is important to note that this curve fit is only valid within the specific range of given nondimensional parameters listed in Table 3.

Based on Eq. (33), assuming other parameters fixed, any decrease in the fluid inlet viscosity causes an increase in the lift-off speed. Physically, a decrease in the fluid inlet viscosity translates

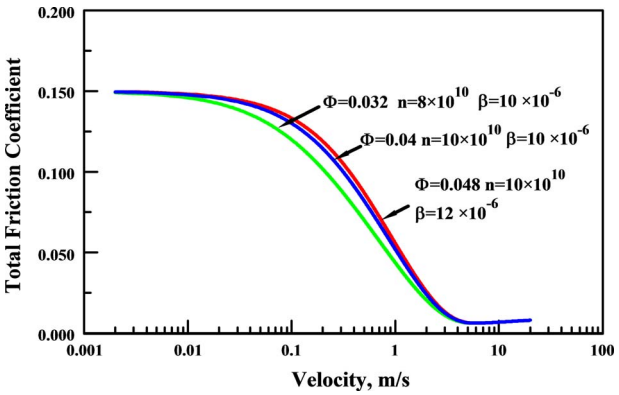

Fig. 8 Total friction coefficient as a function of velocity (roughness effect), $\sigma_s=0.04$ μm and $F_T=40$ N

Table 3 Input parameters for parametric study simulations

Parameter		Range	
W	Load parameter	1.1×10^{-7}	2.1×10^{-5}
G	Material parameter	750	4500
μ	Roughness parameter	2.9	6.05
$U_{\Sigma_{\text{lift-off}}}$	Velocity parameter	3×10^{-11}	9×10^{-11}

to more metal-to-metal contact and higher friction coefficient; this delays the transition from mixed- to full-film-lubrication, which means a high value for the lift-off speed. This is revealed in Fig. 5 comparing Stribeck curve for different oil inlet viscosities. Similarly, an increase in the load parameter will cause a slight increase in the lift-off speed. Figure 6 shows the differences in Stribeck curve for different surface roughnesses. It is clear that for a rougher surface the transition from mixed to full-film regime will occur at a higher speed. This is in agreement with the proposed relation for lift-off speed; nondimensional surface roughness parameter μ will increase due to an increase in the surface roughness, which results in an increase in the lift-off velocity. Some numerical examples are presented in Table 4 and show the comparison of lift-off speed using the proposed relation and full simulations' result. Hundreds of simulations were performed to test the accuracy of Eq. (33) in comparison to full simulations, and the average error was only 0.76%. However, there existed isolated cases with large errors, caused by curve fitting, as shown in Table 4. These are typically when dealing with high G and midrange of μ values. Nevertheless, Eq. (33) is thought to be useful for quick estimation of the lift-off speed.

6 Conclusions

A simple, but realistic model is proposed to predict the behavior of friction coefficient in point contact. The behavior of friction coefficient, when plotted as a function of velocity, reduces to what tribology literature refers to as Stribeck curve. The load-sharing concept is applied to simplify the problem of sliding lubricated contact to dry contact of two spheres and lubricated contact of two smooth spheres. For the contact of two rough spheres, a set of function curve fits has been developed, which can be used to easily predict the load-carrying capacity associated with the asperities. The simulation results are in good agreement with the published experimental data. A parametric study is conducted investigating the influence of different parameters in the behavior of friction coefficient. Parametric study of the model can be useful for design purposes predicting the friction coefficient behavior depends on the operating condition. The proposed model can be used in the design of control algorithm in real-time applications because it is very efficient in terms of computational time and does not encounter numerical stability problems. Based on a series of simulation results under various operating conditions, a relation is proposed to predict the lift-off speed in sliding lubricated point contact with provision for surface roughness.

Nomenclature

A_H = contact area of the fluid, m^2
A_{C_i} = area of an individual asperity in contact, m^2
a = radius of point contact, m
c_p = constant in Eq. (12), 1.962×10^8, Pa
D = ratio of reduced radii of curvature of mating surfaces, $=R_x/R_y$
d_d = distance between mean line of asperities and mean line of surface, m
E = modulus of elasticity, Pa
E' = equivalent modulus of elasticity, $=2[(1-\upsilon_1^2)/E_1+(1-\upsilon_2^2)/E_2]$, Pa
F_f = total friction coefficient
$F_{f,H}$ = hydrodynamic friction force, N
$F_{f,C}$ = asperity contact friction force, N
F_C = asperity interacting force, N
F_H = hydrodynamic lifting force, N
F_T = applied load, N
f = total friction coefficient
f_c = average asperity friction coefficient
h = film thickness, m
h_c = central film thickness, m
k = aspect ratio of the contact ellipse, $=a_x/a_y$
N = number of asperities in contact
n = density of asperities, $1/m^2$
p_c = contact pressure of an asperity in the center of point contact, Pa
p_m = mean pressure of Hertzian contact, Pa
p_H = hydrodynamic pressure, Pa
p_C = asperity contact pressure, Pa
p_T = total pressure, Pa
p_0 = maximum Hertzian pressure for point contact, Pa
R = reduced radius of curvature, $=1/(1/R_1+1/R_2)$, m
u = effective velocity, m/s
Z = pressure-viscosity index
α = pressure-viscosity coefficient, 1/Pa
β = average radius of asperities, m
β_0 = slope of limiting shear stress-pressure relation
γ_1 = hydrodynamic scaling factor
γ_2 = asperity contact scaling factor
$\dot{\gamma}$ = shear stain rate, 1/s
ψ = dimensionless speed parameter
η = dynamic viscosity, Pa s

Table 4 Lift-off speed (Simulations versus Eq. (33))

$W\times10^6$	G	μ	$U_{\Sigma_{\text{lift-off}}}\times10^{11}$ Eq. (33)	$U_{\Sigma_{\text{lift-off}}}\times10^{11}$ simulation	Abs. residual	Error percentage (%)
6.67	2250	3.58	3.6978	3.3813	0.3165	9.36
6.67	3000	3.58	2.9167	3.7152	0.7984	21.49
2.67	1410	3.57	5.3484	5.3088	0.0396	0.746
1.3699	2058.6	3.57	3.8708	3.8846	0.0137	0.355
20.4762	1974	2.9814	3.1930	3.1857	0.0073	0.2306
12.8571	1974	2.9	3.17	3.168	0.003	0.103
5.7143	1974	3	3.205	3.2	0.003	0.11
1.3699	2058	3.6	3.876	3.8708	0.004	0.117
2.1053	1786	3	4.3554	4.38	0.028	0.64
10	1974	2.99	3.1571	3.154	0.002	0.075
1.8182	2068	3.8	3.8393	3.874715	0.035	0.9224

η_0 = inlet dynamic viscosity at zero pressure and room temperature, Pa s
η_∞ = constant in Eq. (12), 6.315×10^{-5} Pa s
Λ = film thickness parameter, $=h_c/\sigma_s$
Φ = surface roughness parameter, $=\sigma_s \beta n$
σ_s = standard deviation of asperities, m
τ_{C_i} = contact shear stress of an individual asperity, Pa
τ_H = fluid shear stress, Pa
τ_L = limiting shear stress, Pa
τ_{L0} = limiting shear stress at ambient pressure, Pa
ν = Poisson ratio

Subscripts

x = x-direction
y = y-direction
1 = body 1
2 = body 2

References

[1] Cheng, H. S., 1970, "A Numerical Solution of the Elastohydrodynamic Film Thickness in an Elliptical Contact," ASME J. Lubr. Technol., **92**(1), pp. 155–162.
[2] Hamrock, B. J., and Dowson, D., 1981, *Ball Bearing Lubrication—The Elastohydrodynamic of Elliptical Contacts*, Wiley-Interscience, New York.
[3] Nijenbanning, G., Venner, C. H., and Moes, H., 1994, "Film Thickness in Elastohydrodynamically Lubricated Elliptic Contacts," Wear, **176**, pp. 217–229.
[4] Greenwood, J. A., and Tripp, J. H., 1967, "The Elastic Contact of Rough Spheres," ASME J. Appl. Mech., **34**(153), pp. 417–420.
[5] Yip, F. C., and Venart, J. E. S., 1971, "An Elastic Analysis of the Deformation of Rough Spheres, Rough Cylinders and Rough Annuli in Contact," J. Phys. D, **4**, pp. 1470–1486.
[6] Zhu, D., and Ai, X., 1997, "Point Contact EHL Based on Optically Measured Three-Dimensional Rough Surfaces," ASME J. Tribol., **119**, pp. 375–384.
[7] Hu, Y.-Z., and Zhu, D., 2000, "A Full Numerical Solution to the Mixed Lubrication Point Contacts," ASME J. Tribol., **122**, pp. 1–9.
[8] Wang, W.-Z., Liu, Y.-C., Wang, H., and Hu, Y.-Z., 2004, "A Computer Thermal Model of Mixed Lubrication in Point Contacts," ASME J. Tribol., **126**, pp. 162–170.
[9] Wang, W.-Z., Wang, S., Shi, F., Wang, Y.-C., Chen, H.-B., Wang, H., and Hu, Y.-Z., 2007, "Simulations and Measurements of Sliding Friction Between Rough Surfaces in Point Contacts: From EHL to Boundary Lubrication," ASME J. Tribol., **129**, pp. 495–501.
[10] Johnson, K. L., Greenwood, J. A., and Poon, S. Y., 1972, "A Simple Theory of Asperity Contact in Elastohydrodynamic Lubrication," Wear, **19**, pp. 91–108.
[11] Gelinck, E. R. M., and Schipper, D. J., 2000, "Calculation of Stribeck Curves for Line Contacts," Tribol. Int., **33**, pp. 175–181.
[12] Liu, Z., Sun, J., and Shen, W., 2002, "Friction of Lubricated Layered Surfaces," Tribol. Trans., **45**(2), pp. 153–160.
[13] Lu, X. B., Khonsari, M. M., and Gelinck, E. R. M., 2006, "The Stribeck Curve: Experimental Results and Theoretical Prediction," ASME J. Tribol., **128**(4), pp. 789–794.
[14] Faraon, I. C., and Schipper, D. J., 2007, "Stribeck Curve for Starved Line Contacts," ASME J. Tribol., **129**, pp. 181–187.
[15] Akbarzadeh, S., and Khonsari, M. M., 2008, "Performance of Spur Gears Considering Surface Roughness and Shear Thinning Lubricant," ASME J. Tribol., **130**(2), p. 021503.
[16] Liu, Q., Napel, W. T., Tripp, J. H., Lugt, P. M., and Meeuwenoord, R., 2009, "Friction in Highly Loaded Mixed Lubricated Point Contacts," Tribol. Trans., **52**(3), pp. 360–369.
[17] Bair, S., and Winer, W. O., 1979, "A Rheological Model for EHL Contacts Based on Primary Laboratory Data," ASME J. Lubr. Technol., **101**, pp. 258–265.
[18] Roelands, C. J. A., 1966, "Correlational Aspects for the Viscosity-Temperature-Pressure Relationship of Lubricating Oils," Ph.D. thesis, University of Technology, Delft, The Netherlands.
[19] Khonsari, M. M., and Booser, E. R., 2008, *Applied Tribology Bearing Design and Lubrication*, Wiley, West Surcek, UK.
[20] Barus, C., 1893, "Isotherms, Isopeistics and Isometrics Relative to Viscosity," Am. J. Sci., **45**, pp. 87–96.
[21] Greenwood, J. A., and Williamson, J. B. P., 1966, "Contact of Nominally Flat Surfaces," Proc. R. Soc. London, Ser. A, **295**, pp. 300–319.